Three-body fragmentation of multiply charged nitrous oxide induced by Ar^{8+}- and Xe^{15+}-ion impact

Arnab Khan, Lokesh C. Tribedi, and Deepankar Misra*

Department of Nuclear and Atomic Physics, Tata Institute of Fundamental Research, Homi Bhabha Road, Colaba, Mumbai 400005, India

(Received 2 March 2017; published 11 July 2017)

We study multiple ionization and subsequent dissociation of nitrous oxide (N_2O) in collisions with 1 a.u. Ar^{8+} and Xe^{15+} ions. The experiments are performed by using a recoil ion momentum spectrometer (RIMS) equipped with a position- and time-sensitive detector which allows the measurement of the momenta of fragment ions in coincidence. By measuring the momentum vectors of the recoiling fragment ions various important parameters, such as kinetic energy release and those related to molecular structure prior to fragmentation, have been derived. Furthermore, the projectile-charge-state dependence of the fragmentation dynamics of N_2O is investigated and a very mild dependence has been noticed in a few channels. In addition, we also study the concerted and sequential mechanisms in the three-body decay of N_2O^{q+} (where $q \leqslant 7$). It has been observed that N_2O^{q+} breaks up mainly in a concerted manner except for the $N_2O^{3+} \rightarrow N^+ + N^+ + O^+$ (1,1,1) and $N_2O^{4+} \rightarrow N^{2+} + N^+ + O^+$ (2,1,1) channels. For both these channels, the presence of an intermediate rotating NO^{2+} has been identified. Furthermore, by using Dalitz plot analysis, we have been able to separate various mutually mixed channels of highly charged N_2O^{q+}.

DOI: 10.1103/PhysRevA.96.012703

I. INTRODUCTION

Three-body dissociation and the associated phenomena of tri- and polyatomic molecules are perhaps one of the most intriguing subjects of physical science and has caught an enormous amount of attention in the last decades [1–4]. Unlike two-body dissociation, the interplay between various internuclear motions, higher numbers of electronic and vibrational degrees of freedom, as well as a manifold of dissociation pathways make the understanding of three-body fragmentation highly complicated for both experiment as well as theory [5,6]. It is also known that the three-body dissociation of a neutral molecule can happen in the stratosphere, interstellar medium, in combustion processes, and in high-energy processes [1]. Alternatively, in the laboratory, when a tri- or polyatomic molecule is exposed to an ionizing medium, such as free-electron lasers [7–9], synchrotron radiation [3], intense femtosecond lasers [10–12], and even highly charged ion beams [2,4,13], it becomes multiply ionized. This sudden expulsion of multiple electrons can, sometimes, lead to the three-body fragmentation of the molecular ion triggered by the mutual Coulomb force.

To date, the energetics and dynamics of the three-body Coulomb explosion process have been studied for several molecular systems starting from the symmetric triatomic molecules such as CO_2 [2,4], CS_2 [3,14], SO_2 [15], and asymmetric molecules such as OCS [16], and even in case of several polyatomic molecules [12,17]. Furthermore, the ionization and fragmentation of N_2O were mainly investigated in photon- [18–20] and electron-impact [21–23] experiments. A large part of the previous work on N_2O has been concentrated, mainly, on the two-body dissociation dynamics [18,20,24,25]. The laser-induced three-body breakup dynamics of N_2O was first studied by Frasinski *et al.* [26], where they identified the $N_2O^{6+} \rightarrow N^{2+} + N^{2+} + O^{2+}$ decay channel by using a three-dimensional covariance mapping technique. Besides, Hishikawa *et al.* have shown various three-body dissociation channels of N_2O^{q+} ($q = 3$–8) following the multiple ionization by intense femtosecond laser (pulse length 100 fs, 795 nm, 5.0 PW/cm^2) [27]. Later, a three-dimensional (3D) coincident momentum spectroscopic study of N_2O was performed by Ueyama *et al.* using 60 fs (800 nm, 0.16 PW/cm^2) laser pulses [28]. In this work, the authors showed the presence of both concerted and sequential channels in the three-body decay of N_2O^{3+}. In recent times, Karimi *et al.* reported the Coulomb explosion phenomena of highly charged N_2O^{q+} ($q = 3$–6) for femtosecond laser pulses [29]. Furthermore, in case of electron impacts, Bhatt *et al.* [22] and Khan *et al.* [23] studied the three-body fragmentation of N_2O for charge states up to 3+. On the other hand, the ion-induced three-body dissociation mechanism of N_2O has received much less attention. The only study available by Werner *et al.* [30] which, however, was performed at very high projectile velocities and is limited to very few dissociation channels. In this paper, we present a detailed momentum spectroscopic study of the three-body fragmentation of N_2O^{q+} for $3 \leqslant q \leqslant 7$ in collisions with highly charged ions. The kinetic-energy release (KER) distributions for various dissociation channels are derived and compared with the pure Coulomb explosion (CE) model as well as with the available data in the literature. Special attention is given to identify the structural deformation along with the concerted and sequential bond-breakage mechanisms for $q \geqslant 3$. In addition, we also discuss the projectile-charge-state dependence of the fragmentation dynamics of N_2O.

II. EXPERIMENTAL DETAILS

The experimental setup used is the same as described earlier [31], therefore we give here only a brief summary. The experiments were carried out at the Electron Cyclotron Resonance based ion accelerator (ECRIA) of the Tata Institute

*dmisra@tifr.res.in

of Fundamental Research (TIFR), Mumbai [32]. In the present experiments, well-collimated (0.8 mm in diameter) beams of 1 a.u. Ar^{8+} (1 MeV) and Xe^{15+} (3.2 MeV) were crossed with an effusive jet of nitrous oxide gas at right angles at the center of the pusher and puller electrodes of the spectrometer [31]. After the interaction, all three ionic fragments are guided onto a two-dimensional position-sensitive detector by static electric fields of about 173 V/cm (extraction field) and 250 V/cm (acceleration field), respectively. On the other hand, ejected electrons are extracted in the opposite direction and detected by a channel electron multiplier (CEM). This CEM signal was used as the start to the data-acquisition electronics. A typical count rate was between 500 and 700 Hz. A RoentDek [33] fast analog-to-digital converter (fADC) was used to record the data. All the data were recorded in event-by-event mode in list-mode-file(s). By measuring the time of flight (ToF) and the detector hit positions (x, y), the three-dimensional momentum vectors for each fragment ion were obtained in the laboratory frame. Specifically, during the data analysis we considered two conditions to be fulfilled; the first condition requires the detection of all the three particles in coincidence, i.e., they are all coming from a single event, and second, we put conditions on the momentum sum of the three fragment ions, in each direction ($p_i = |p_{1i} + p_{2i} + p_{3i}|$, where $i = x, y, z$), to be less than 15 a.u. to satisfy momentum conservation. This is a reasonable approximation if we consider that the magnitude of the momentum carried by the emitted electrons is much smaller than that of the fragment ions. Typical base pressure in the scattering chamber was kept around 2×10^{-8} mbar, while during the experiments the operating pressure was around 2×10^{-7} mbar.

III. RESULTS AND DISCUSSIONS

A. Dissociation of N_2O^{3+} and N_2O^{4+}

From the measured momenta of the coincidentally detected fragment ions, the KER distributions for the different dissociation channels are obtained. In this paper, we present the KER distributions for 13 three-body fragmentation channels of N_2O^{q+} for charge states from 3+ to 7+, where all the fragments are charged. Therefore, we start our discussion by studying the KER spectra of N_2O^{3+} ion. Figure 1(a) shows the KER spectra of the $N_2O^{3+} \rightarrow N^+ + N^+ + O^+$ (1,1,1) channel for Ar^{8+}- and Xe^{15+}-ion impacts. For both projectiles, we observe that the KER distributions peak around a KER value of 24.5 eV and having a KER-width about 23.0 eV (from 17.0 to 40.0 eV). The KER spectra, furthermore, have been compared with the KER value obtained from the CE model which predicts a KER value around 31.0 eV for this channel. In this model the KER value can be obtained by using the following equation:

$$\mathrm{KER}_{CE}\ (\text{in eV}) = 14.4 \sum_{i<j} \frac{q_i q_j}{r_{ij}}, \tag{1}$$

where particles are considered as point charges (q_i and q_j) with a separation r_{ij} (in Å) between them. In addition, the model also assumes that r_{ij} is the equilibrium internuclear distance R_e of the neutral molecule [for N_2O, R_e(N-N) $\sim$ 1.13 Å and R_e(N-O) $\sim$ 1.19 Å [27]]. In the case of our previously published electron-impact data, the mean KER value was found around 28.0 eV for this channel [23] while the ion impact study by Werner *et al.* shows the KER distributions peak around the same value (32.0 eV) for different fast highly charged projectiles [30]. Furthermore, as one can see, for this channel and few other decay channels the KER distributions are little asymmetric (cf. Figs. 1 and 3). This means that the most probable KER values are less than the mean KER values and dissociation is happening at longer internuclear distances than the average ones. Therefore, we also calculate the mean value of the KER distributions for all the channels and a comparison of all these values (most probable values, mean values, and CE predictions) is done in the Table I. Here we notice for highly asymmetric channels, in terms of KER distributions, the mean value of the KER distributions match better with the CE predictions. On the other hand, after quadruple ionization, the N_2O^{4+} ion can decay via two channels: $N^{2+} + N^+ + O^+$ and $N^+ + N^+ + O^{2+}$.

Figure 1(b) shows the KER spectra for $N_2O^{4+} \rightarrow N^{2+} + N^+ + O^+$ channel along with the predictions of the CE model (shown by a vertical line and a downward-pointing arrow). Both the spectra have a peak around 39.0 eV followed by a tail-like distribution extending up to 75.0 eV. The possible origin of this long tail-like distribution in the high KER side [cf. Figs. 1(a) and 1(b)] can be the fragmentation of different ionic states via conical intersection ("curve-crossing" in the two-dimensional case) [34,35]. In Fig. 1(b) we also show two KER values (vertical line and downward-pointing

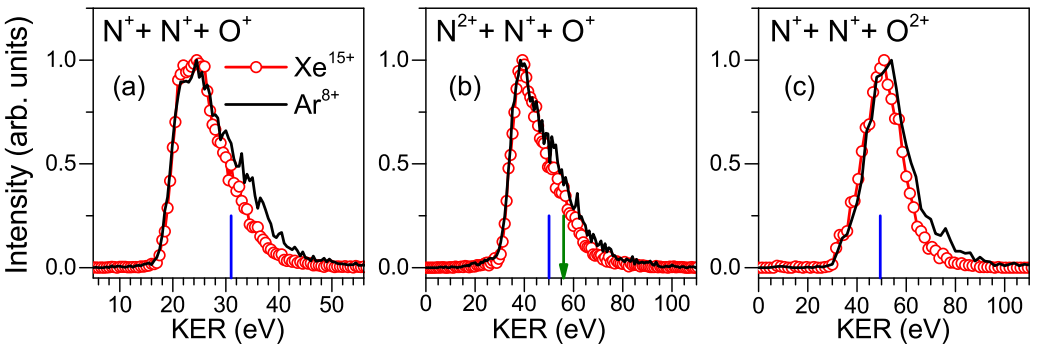

FIG. 1. Kinetic-energy release distributions of N_2O^{3+} and N_2O^{4+} molecular ions fragmenting into (a) $N^+ + N^+ + O^+$, (b) $N^{2+} + N^+ + O^+$, and (c) $N^+ + N^+ + O^{2+}$ channels for Ar^{8+} and Xe^{15+} projectiles. The vertical lines and arrow show predictions of the CE model (see text for details).

TABLE I. Measured kinetic-energy release for the three-body decay of N_2O^{q+} ($q \leqslant 7$) together with the predictions by Coulomb explosion model and the experimental data of Werner *et al.* (projectile: 5.9 MeV/u Xe^{18+}) [30].

Channel N_t-N_c-O	KER (eV) Present experiment (Xe^{15+}) Most probable value	KER (eV) Present experiment (Xe^{15+}) Mean value	KER (eV) CE	KER (eV) Werner *et al.* [30]
(1,1,1)	22.0, 24.5	27.0	31.0	~32.0
(2,1,1)	39.0	45.0	50.0	
(1,2,1)	44.0	47.0	56.0	~53.0
(1,1,2)	51.0	51.0	49.4	
(2,2,1)	75.0	80.0	87.6	~84.0
(2,1,2)	74.0	77.0	74.5	
(1,2,2)	84.0	85.0	86.3	
(3,1,1)	76.0	79.0	68.9	
(1,3,1)	80.0	87.0	80.7	
(1,1,3)	76.0	79.0	67.7	
(2,1,3)	106.0	115.0	99.0	
(1,2,3)	117.0	123.0	116.7	
(2,2,2)	112.0	117.0	124.2	~116.0
(3,2,1)	108.0	112.0	119.3	
(2,3,1)	112.0, 124.0	117.0	125.2	
(3,1,2)	105.0	111.0	99.7	
(1,3,2)	123.0	127.0	123.2	
(2,2,3)	155.0	159.0	160.8	
(3,2,2)	152.0	149.0	162.1	
(2,3,2)	152.0	164.0	173.9	

arrow) as the CE model prediction for N_2O^{4+}; this is because, for this channel, N_2O^{4+} can decay via $N_t{}^{2+} + N_c{}^{+} + O^{+}$ [(2,1,1); expected KER from the CE model is 50.0 eV (line)] and $N_t{}^{+} + N_c{}^{2+} + O^{+}$ [(1,2,1); expected KER from the CE model is 56.0 eV (downward-pointing arrow)] pathways. Here, N_t stands for the terminal nitrogen atom and N_c for the central nitrogen atom of N_2O molecule. A detailed discussion on these channels will be presented later in this section and in Sec. III C.

The KER spectra for the $N_2O^{4+} \rightarrow N^{+} + N^{+} + O^{2+}$ (1,1,2) channel are shown in Fig. 1(c). It can be seen that the KER distributions peak around 54.0 eV (for Ar^{8+}) and 51.0 eV (for Xe^{15+}), which are a little bit higher than the CE prediction (49.4 eV). We found the branching ratio of [(2,1,1) + (1,2,1)] and (1,1,2) channels to be 0.75 : 0.25 in the present experiment. In addition, no distinctive charge-state dependence has been observed in the KER spectra of N_2O^{3+} and N_2O^{4+} for different projectiles [cf. Figs. 1(a)–1(c)]. Furthermore, we have extended our study to investigate possible concerted (single-step) and sequential (two-step) decay channels for N_2O^{3+} and N_2O^{4+}. In our previous study, with electrons, we showed the presence of a sequential decay channel in the case of N_2O^{3+} (1,1,1) [23]. On the other hand, in case of fast electrons, unlike ion impacts, the population of the N_2O^{4+} molecular ion was negligibly less. Here we have used the similar analysis procedure to mark the central (N_c) and terminal (N_t) nitrogen atom as it was done in our earlier publication [23]. Therefore, in this manuscript we will not discuss the analysis procedure for the (1,1,1) channel. Moreover, we use the Dalitz plots [36] and Newton diagrams [4] to visualize the concerted and sequential mechanisms in much detail. In a Dalitz plot the x and y axes are defined as $x_D = (\epsilon_1 - \epsilon_2)/\sqrt{3}$ and $y_D = \epsilon_3 - 1/3$, respectively. Here, $\epsilon_i = |p_i|^2/\sum_i |p_i|^2$ and p_i is the momentum of the ith fragment ion in the center-of-mass frame where $i = N^{a+}$, N^{b+}, and O^{c+}. Figure 2(a) shows the Dalitz plot for the (1,1,1) channel where we see an intense distribution near $(x_D, y_D) = (0.00, -0.33)$ representing the concerted decay process ($N_2O^{3+} \rightarrow N_t{}^{+} + N_c{}^{+} + O^{+}$). Along with that one can also notice a trace of particle distribution to the right side of the $x_D = 0$ line ($x_D = 0.00$ to 0.33 and $y_D = -0.33$ to 0.25) which corresponds to the sequential process, $N_2O^{3+} \rightarrow N_t{}^{+} + N_cO^{2+} \rightarrow N_t{}^{+} + N_c{}^{+} + O^{+}$. However, in the present experiment, we do not see the signature of the other sequential channel $N_2O^{3+} \rightarrow N_2{}^{2+} + O^{+} \rightarrow N^{+} + N^{+} + O^{+}$. This may be due to a very short lifetime of the intermediate excited $N_2{}^{2+}$ molecular ion which breaks before any kind of rotation [23,28]. Furthermore, we cannot rule out another possibility of not observing this sequential channel, i.e., for some of the events it is also possible to make the wrong assignment between N_t and N_c due the mixture with concerted processes [23,28].

The Dalitz plot for the (2,1,1) + (1,2,1) channels is shown in Fig. 2(d), where one can see an intense distribution around $(x_D, y_D) = (0.05, -0.33)$ along with a wing-like structure to the right side of the $x_D = 0$ line. This intense distribution of particles comes from the concerted decay of the $N_2O^{4+} \rightarrow N_t{}^{2+} + N_c{}^{+} + O^{+}$ (2,1,1) with a little asymmetric geometry. While the wing-like structure has its origin from the sequential decay of N_2O^{4+} into $N_t{}^{2+} + N_c{}^{+} + O^{+}$ via the $N_t{}^{2+} + N_cO^{2+}$ channel. Furthermore, in Fig. 2(d) we notice another distribution of particles around $(x_D, y_D) = (-0.30, 0.20)$. Here is an interesting thing to be noticed, the particles are distributed, mostly, near the region where N^{2+} line intersects the circle and triangle. This indicates for these particles N^{+} and O^{+} take away most of the kinetic energy

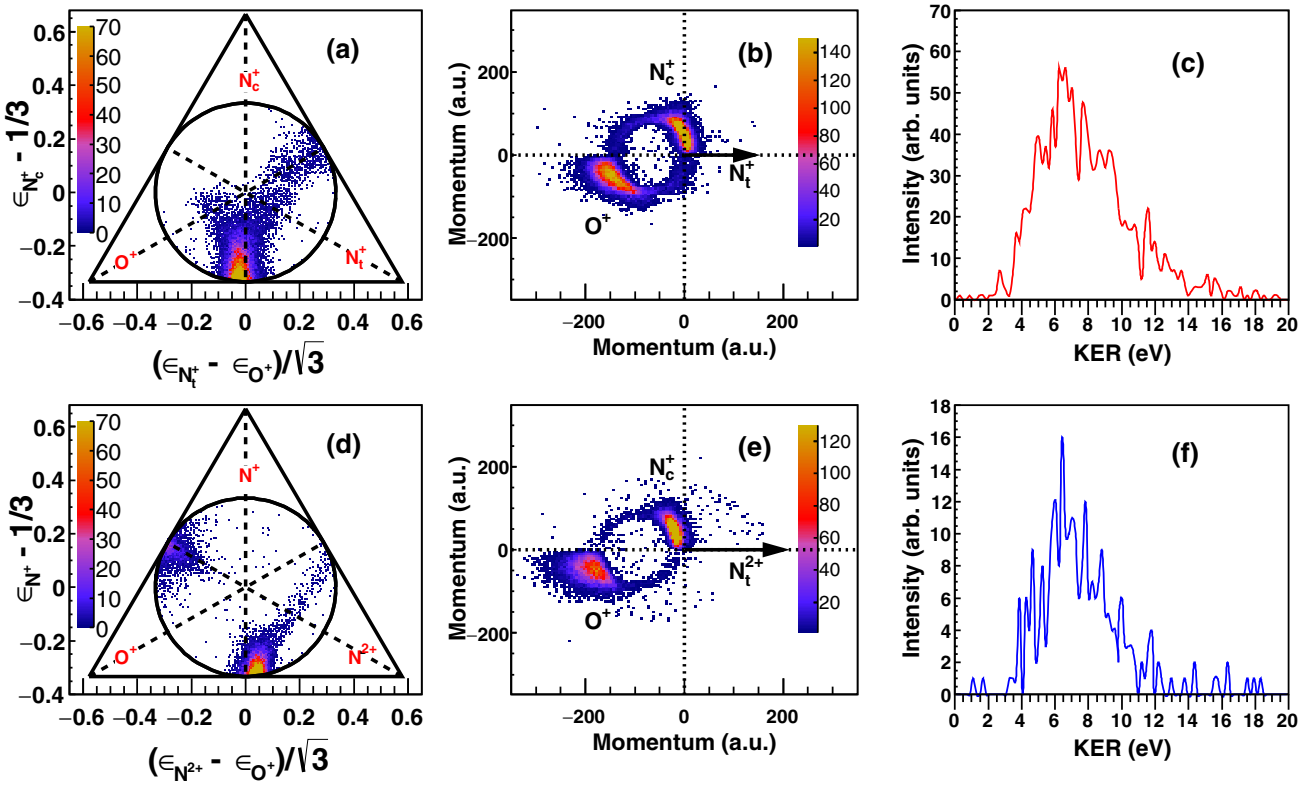

FIG. 2. (a) Dalitz plot for $N_2O^{3+} \rightarrow N^+ + N^+ + O^+$ (1,1,1) channel in collision with and Xe^{15+} ion impacts. (b) Newton diagram for N_2O^{3+} (1,1,1) channel. Here, semicircular structures show the sequential decay whereas two crescent-like structures represents the concerted decay. (c) KER distribution of $N_cO^{2+} \rightarrow N_c^+ + O^+$ sequential decay channel for N_2O^{3+} (1,1,1). (d) Dalitz plot for $N_2O^{4+} \rightarrow N^{2+} + N^+ + O^+$ [(2,1,1) + (1,2,1)] decay induced by Xe^{15+} ion. (e) Newton diagram for (2,1,1) channel. (f) KER distribution for $N_cO^{2+} \rightarrow N_c^+ + O^+$ sequential decay of (2,1,1) channel.

(KE), leaving N^{2+} with much less KE, and fragmentation is happening in a near-symmetric geometry. This is only possible if N^+ is terminal and N^{2+} is central. Thus, we can easily conclude that this distribution is coming from the decay of N_2O^{4+} via $N_t^+ + N_c^{2+} + O^+$ (1,2,1) channel. A more detailed discussion on the separation of these mutually mixed channels will be done in Sec. III C. The Newton diagram for the $N_2O^{3+} \rightarrow N_t^+ + N_cO^{2+} \rightarrow N_t^+ + N_c^+ + O^+$ (1,1,1) channel is shown in Fig. 2(b), whereas the Newton diagram for the $N_2O^{4+} \rightarrow N_t^{2+} + N_cO^{2+} \rightarrow N_t^{2+} + N_c^+ + O^+$ (2,1,1) channel is shown in Fig. 2(e). In the Newton diagrams we have plotted the momentum of $N_t^{+/2+}$ along the x axis whereas the momentum of N_c^+ and O^+ parallel and perpendicular to the $N_t^{+/2+}$ are plotted in the +ve and −ve y axis. In each plot the arrow sign indicates the most probable value of the momentum distribution of $N_t^{+/2+}$ ions along the x axis. Both the Newton diagrams show a clear signature of the rotation of the intermediate N_cO^{2+} molecular ions. In addition, we also show the KER for the second breakup channels, i.e., $N_cO^{2+} \rightarrow N_c^+ + O^+$, in Figs. 2(c) and 2(f) for both (1,1,1) and (2,1,1) channels. These spectra have been generated by setting conditions on the sequential part of the Dalitz plots [Figs. 2(a) and 2(d)] and going into the center-of-mass (c.m.) frame of N_cO^{2+}. The resulting KER distribution extends from 2.0 to 14.0 eV and has its maximum at about 6.4 eV for both the cases. On the other hand, the radii of the semicircular distributions in the Newton diagram correspond to a mean KER value of 7.0 eV for these channels. By comparing with the literature we can say that these KER spectra correspond to $X^2\Sigma^+$, $A^2\Pi$, $B^2\Sigma^+$, $C^2\Sigma^+$, and $c^4\Pi$ states of NO^{2+} molecular ion [37–39]. Here, it will be compulsive to mention that, in the present case, for (1,1,1) channel we found the branching ratio of the sequential decay process to be around 12%–13% of the total number of events. Moreover, analysis of the Newton diagram reflects that, for this sequential decay, the expected KER is about 24 eV (for similar analysis-details see Ref. [4]). Whereas, for N_2O^{4+}, the sequential decay routes [(2,1,1) + (2,1,2)] contribute about 6%–7% of the total events and the expected KER is around 36 eV. Therefore, although the contributions from the sequential decay channels are very small fractions of the total number of events, the possibility of lowering of total KERs to a much lower value than the CE predictions cannot be ruled out completely owing to the presence of the sequential decay channels for these two decay routes.

B. Kinetic-energy release spectra of N_2O^{q+} ($5 \leqslant q \leqslant 7$)

We have seen four three-body decay channels in the dissociation of N_2O^{5+}, and the KER spectra for all these dissociation channels are shown in Figs. 3(a)–3(d). Among these, as a first example, we plot the KER spectra for the $N_2O^{5+} \rightarrow N^{2+} + N^{2+} + O^+$ (2,2,1) in Fig. 3(a) along with the

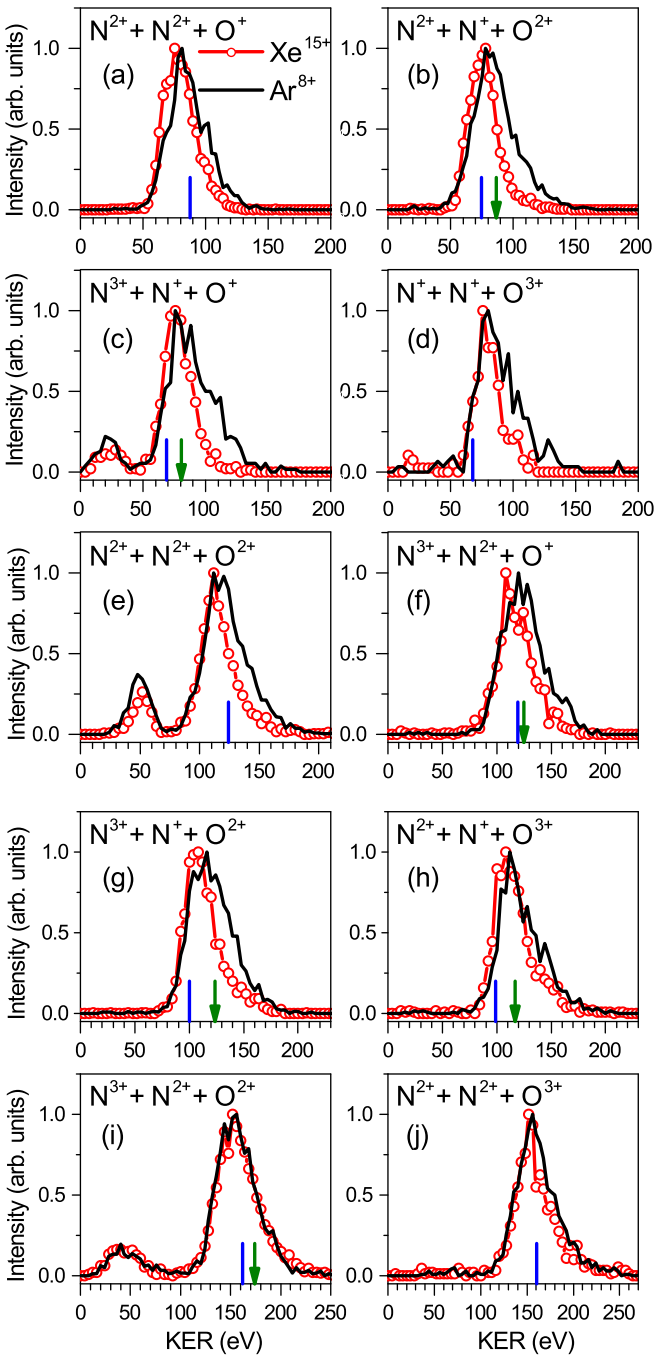

FIG. 3. (a)–(j) Total kinetic-energy release distributions of $N_2O^{q+} \rightarrow N^{a+} + N^{b+} + O^{c+}$ $(q = a + b + c)$ fragmentation in collisions with 3.2 MeV Xe^{15+} and 1.0 MeV Ar^{8+} ions and corresponding kinetic-energy release prediction(s) of the CE model are shown by vertical lines and down arrows. Here, vertical line represents the $N_2O^{q+} \rightarrow N^{a+} + N^{b+} + O^{c+}$ decay when $a > b$, whereas down arrow stands for the decay with $b > a$.

KER value predicted by the CE model (vertical line). From the figure it can be seen that the peak values of the experimental KER spectra (75.0 eV for Xe^{15+} and 81.0 eV for Ar^{8+}) are lower than the CE predicted value (87.6 eV). Furthermore, the Dalitz plot (not shown in the paper) reveals that the decay of N_2O^{5+} into $N^{2+} + N^{2+} + O^{+}$ happens only via concerted process with a little asymmetric geometry. Besides, N_2O^{5+} can also decay by means of a second channel: $N_2O^{5+} \rightarrow N^{2+} + N^{+} + O^{2+}$. The KER spectra and CE predictions for this channel are shown in Fig. 3(b). Both the KER spectra are observed to peak at 78.0 eV. It is also seen that the width of the spectra for the impact of Xe^{15+} is sharper than that of Ar^{8+}. A similar type of dependence on projectile charge state has been observed previously in the case of $CO^{2+} \rightarrow C^{+} + O^{+}$ dissociation by Folkerts *et al.* in collision with He^{2+} and O^{7+} (4 keV/amu in both the cases) [40]. Where the authors had concluded that, in the case of He^{2+}, higher excited states of the CO^{2+} molecular ion are getting populated. Moreover, in the case of highly charged ion impacts, electron transfer as well as transfer ionization processes can take place at large impact parameters. Therefore, for a more highly charged projectile ion (in their case O^{7+}), during ionization, energy deposition to the system is low compared with a less charged projectile and as a result KER can also be low [40]. A similar dependence was also noticed in case of N_2 ionization and the dependence on projectile charge states was explained by considering the population in different excited states of the intermediate molecular ion [41]. We expect that these arguments may also hold for N_2O fragmentation. But Figs. 1 and 3 show that this dependence is seen for few channels of intermediate charge states and, therefore, to conclude something more specifically, more detailed experimental and theoretical investigations are necessary. Now this final state can arise from two different decay routes: $N_2O^{5+} \rightarrow N_t{}^{+} + N_c{}^{2+} + O^{2+}$ [(1,2,2); CE predicted KER: 86.3 eV], and $N_2O^{5+} \rightarrow N_t{}^{2+} + N_c{}^{+} + O^{2+}$ [(2,1,2); CE predicted KER: 74.5 eV] channels which are mixed in the present KER spectra shown in Fig. 3(b). These two channels, however, can be separated by the Dalitz plot analysis and this will be addressed in the next section. The KER spectra for the $N_2O^{5+} \rightarrow N^{3+} + N^{+} + O^{+}$ decay channel are shown in Fig. 3(c). Here we see the most probable value of the KER is around 76.0 eV. Moreover, for this channel also the width of the KER spectra show some dependence on the projectile charge state. Along with that, we also see a small but prominent distribution around 20.0 eV. This low-energy peak may originate from the predissociation of N_2O^{5+} molecular ion [35]. Another possibility could be dissociation via a secondary decay process, such as atomic autoionization, where the autoionization happens at a large distance from the equilibrium distance. But to make any further comments, an energy-analyzed electron-ion coincidence measurement is necessary. Furthermore, the KER spectra for the $N_2O^{5+} \rightarrow N^{+} + N^{+} + O^{3+}$ (1,1,3) channel are shown in Fig. 3(d) along with the KER value expected by the CE model. Similar to the $N_2O^{4+} \rightarrow N^{+} + N^{+} + O^{2+}$ (1,1,2) channel, here also, it can be seen that the peak value of our experimental KER distributions are higher than the value estimated by the CE model. Moreover, for this channel the Dalitz-plot analysis reveals that the decay of N_2O^{5+} molecular ions occurs only via a concerted channel with a highly asymmetric geometry (not shown in the paper). And the branching ratios of all these fragmentation channels are found to be $[(2,1,2) + (1,2,2)] : (2,2,1) : [(3,1,1) + (1,3,1)] : (1,1,3) = 0.58 : 0.34 : 0.05 : 0.03$.

On the other hand, in the present experiment, four dissociation channels have been observed in the decay of N_2O^{6+} ion, and the KER spectra for these decay channels

are shown in Figs. 3(e)–3(h). First of all, we choose the totally symmetric and the most dominant channel $N_2O^{6+} \rightarrow N^{2+} + N^{2+} + O^{2+}$ (2,2,2). The KER distributions for this channel are shown in Fig. 3(e). For Xe^{15+} impacts the KER distribution peaks around the KER value of 112.0 eV, whereas for Ar^{8+} ion impacts one can easily identify two peaks around 112.0 and 120.0 eV, respectively (the CE model predicted KER is 124.2 eV). Additionally, both the KER spectra show another small peak around 50.0 eV (similar to the $N_2O^{5+} \rightarrow N^{3+} + N^+ + O^+$ channel) and the width of this peak has no dependence on the projectile charge states. Figure 3(f) shows the KER spectra for the $N_2O^{6+} \rightarrow N^{3+} + N^{2+} + O^+$ decay channel. For Xe^{15+} ion impacts the KER distribution peaks around 108.0 and 124.0 eV. While in case of Ar^{8+} ions one can identify two peaks around 120.0 and 128.0 eV. The KER distributions for $N_2O^{6+} \rightarrow N^{3+} + N^+ + O^{2+}$ and $N_2O^{6+} \rightarrow N^{2+} + N^+ + O^{3+}$ channels are shown in Figs. 3(g) and 3(h), respectively. It can be seen that the KER spectra for $N_2O^{6+} \rightarrow N^{3+} + N^+ + O^{2+}$ channel very weakly depend on projectile charge state whereas $N_2O^{6+} \rightarrow N^{2+} + N^+ + O^{3+}$ channel seems to be independent of projectile charge state. Furthermore, in the case of N_2O^{6+} decay, the branching ratios of the various decay channels are found to be (2,2,2) : [(3,1,2) + (1,3,2)] : [(2,1,3) + (1,2,3)] : [(3,2,1) + (2,3,1)] = 0.43 : 0.26 : 0.19 : 0.12.

For the decay of N_2O^{7+} we have seen only two channels with sufficient statistics. These two channels are $N_2O^{7+} \rightarrow N^{3+} + N^{2+} + O^{2+}$ [(3,2,2) + (2,3,2)] and $N_2O^{7+} \rightarrow N^{2+} + N^{2+} + O^{3+}$ [(2,2,3)], respectively. The KER spectra for the $N_2O^{7+} \rightarrow N^{3+} + N^{2+} + O^{2+}$ decay channel are shown in Fig. 3(i). An additional small distribution can be seen around 40.0 eV along with the main KER distribution (peaks around 152.0 eV). Lastly, the KER spectra for the (2,2,3) decay channel are shown in Fig. 3(j). For both the projectiles the KER spectra have a peak around 155.0 eV and the most probable value of the KER spectra is very close to the prediction by the CE model (the CE model predicts a KER value of 160.8 eV for this channel) and it is also seen that the width of the KER spectra do not exhibit any projectile-charge-state dependence. We found the experimental branching ratio of the these two channels to be [(3,2,2) + (2,3,2)] : (2,2,3) = 0.63 : 0.37. Here, it is worth mentioning that, for some of the channels, such as (2,2,1), (1,1,3), (2,2,2), and (2,2,3), the present branching ratios will be little lower due dead-time effect of the detector and data-acquisition electronics [31]. Along with that, we have also seen, sometimes, this loss can be up to 15%. Table I summarizes the KER values for different three-body breakup channels of N_2O^{q+} (q = 3–7; here we have shown Xe^{15+} impacts data only) along with a few experimental KER values provided by Werner *et al.* [30], including the KER values estimated by the CE model.

C. Kinetic-energy release spectra with condition on Dalitz plot

In Sec. III A we describe that, considering the energy correlation among the particles, one can easily distinguish between the (2,1,1) and (1,2,1) channels of $N_2O^{4+} \rightarrow N^{2+} + N^+ + O^+$ by using the Dalitz plot. This can be treated as a great advantage of the Dalitz plot analysis by which one can

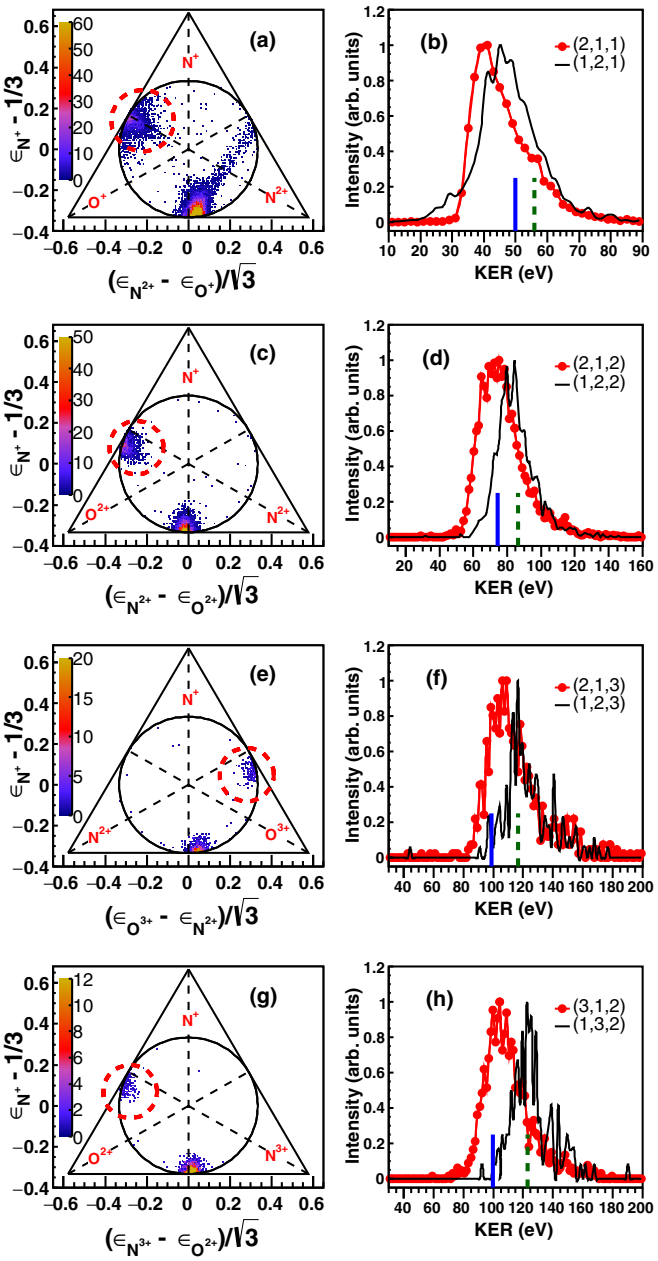

FIG. 4. (a)–(h) Dalitz plots and corresponding KER spectra for different three-body fragmentation channels of N_2O^{q+}. Figures in the right panel show the KER spectra for different mutually mixed decay channels, while figures in the left panel show the total Dalitz plots of these channels. The red dashed circles in the Dalitz plots indicate the decay channels: $N_2O^{q+} \rightarrow N^{a+} + N^{b+} + O^{c+}$ decay where $b > a$.

easily separate out the two mutually mixed decay channels by examining the energy correlations. The condition on the Dalitz plot for N_2O^{4+} is shown in Fig. 4(a) where the (1,2,1) channel is shown by a red dotted circle. Now, by using this condition we plotted the KER spectra for the $N_t^{2+} + N_c^+ + O^+$ (2,1,1) and $N_t^+ + N_c^{2+} + O^+$ (1,2,1) channels along with the CE predictions [50.0 eV for (2,1,1) and 56.0 eV for (1,2,1); shown by vertical solid line and dotted line] in Fig. 4(b). Our KER spectra also show clear difference between the most probable KER values for these channels, although present

values [39.0 eV for (2,1,1) and 44.0 eV for (1,2,1)] are lower than the CE predicted values. However, the difference in the KER values for these two channels (i.e., 6.0 eV) matches quite well with the CE model. To separate out these two channels a similar analysis procedure was previously used by Karimi *et al.* and they found the KER values of (2,1,1) and (1,2,1) to be ∼29.0 eV and ∼34.0, respectively [29]. Furthermore, the branching ratio of (2,1,1) and (1,2,1) channels is found to be 0.863 : 0.137. As discussed earlier in Sec. III B, $N_2O^{5+} \rightarrow N^{2+} + N^+ + O^{2+}$ actually decays via two mutually mixed channels: $N_2O^{5+} \rightarrow {N_t}^+ + {N_c}^{2+} + O^{2+}$ (1,2,2), and $N_2O^{5+} \rightarrow {N_t}^{2+} + {N_c}^+ + O^{2+}$ (2,1,2). The CE model expected KER for the (1,2,2) channel is 86.3 eV and for the (2,1,2) channel it is 74.5 eV. The experimental KER spectra for these two channels are shown in Fig. 4(d) along with Dalitz plot [cf. Fig. 4(c)]. We notice that the experimental KER spectra show a clear difference between two decay channels with the most probable KER at 74.0 eV for (2,1,2) (vertical solid line) and 84.0 eV for (1,2,2) (vertical dotted line) channels. Moreover, no sign of the sequential decay has been observed in these decay channels. The Dalitz plot also shows for the (2,1,2) channel that the molecule breaks symmetrically, while for the (1,2,2) channel an asymmetric bond breakage is most probable. Furthermore, the branching ratio of these two channels is found as (2,1,2) : (1,2,2) = 0.667 : 0.333.

Figure 4(e) shows the Dalitz plot for the $N_2O^{6+} \rightarrow N^{3+} + N^+ + O^{2+}$ channel. Here, the mutually mixed decay channels are (2,1,3) and (1,2,3). Now in the Dalitz plot one can see two blobs of particle distribution: one near $x_d = 0.0$ and another one on the right side of the $x_d = 0.0$ line (i.e., the N^+ line). A careful observation reveals that the distribution near $x_d = 0.0$ originates from $N_2O^{6+} \rightarrow {N_t}^{2+} + {N_c}^+ + O^{3+}$ (2,1,3). For this channel, ${N_t}^{2+}$ and O^{3+} takeaway most of the KE and N_2O^{6+} breaks in a slightly asymmetric geometry. On the other hand, the other distribution comes from the $N_2O^{6+} \rightarrow {N_t}^+ + {N_c}^{2+} + O^{3+}$ (1,2,3) channel and for this channel the molecular ion breaks apart in strongly asymmetric manner. The KER spectra for these two channels are shown in Fig. 4(f) and the KER distributions follow the same trend expected by the CE model (for KER values see Table I). The branching ratio of (2,1,3) and (1,2,3) channels is found to be 0.805 : 0.195. Now N_2O^{6+} via the $N^{3+} + N^+ + O^{2+}$ channel can originate from the decay routes of N_2O^{6+} via the ${N_t}^{3+} + {N_c}^+ + O^{2+}$ (3,1,2) and ${N_t}^+ + {N_c}^{3+} + O^{2+}$ (1,3,2) channels. The CE model predicts quite different KER values for these two decay channels [for the (3,1,2) channel the expected KER is 99.7 eV and for the (1,3,2) channel the KER is 123.2 eV]. So the evaluation of the experimental KER by the Dalitz plot technique will be a very good test for the scheme we have used so far to find the KER for the two mutually mixed channels. To this end, we plot the KER distributions [cf. Fig. 4(h)] by selecting the proper regions in the Dalitz plot [shown in Fig. 4(g)] and we see two KER distributions with the most probable KER values of 105.0 eV [for the (3,1,2) channel] and 123.0 eV [for the (1,3,2) channel]. This observation, in turn, strengthens the scheme used to separate two mutually mixed channels. The experimental branching ratio for these two channels is (3,1,2) : (1,3,2) = 0.883 : 0.117.

In addition, we also investigate another three channels where mutually mixed channels are present. But for these channels, either the data suffer from low statistics or the CE model expected energies are not sufficiently well separated to display a substantial difference in the experimental KER spectra. Therefore, keeping these in mind, the plots for these three channels will not be presented in the paper, but the observed KER values are presented in Table I. Among these, first we study the decay of N_2O^{5+} via the $N_2O^{5+} \rightarrow {N_t}^{3+} + {N_c}^+ + O^+$ (3,1,1) and $N_2O^{5+} \rightarrow {N_t}^+ + {N_c}^{3+} + O^+$ (1,3,1) channels by putting a condition on the Dalitz plot (in this case the Dalitz plot is drawn only for the high-energy part of the KER distribution). The experimental KER spectra also show some difference for the (3,1,1) and (1,3,1) channels. But due to low statistics in the (1,3,1) channel, at present, it is very difficult find the exact peak value for this channel. However, the KER spectra show a similar trend as expected from the CE model. The branching ratio for these channels is found to be (3,1,1) : (1,3,1) = 0.943 : 0.057. Furthermore, the dissociation of N_2O^{6+} into the ${N_t}^{2+} + {N_c}^{3+} + O^+$ (2,3,1) and ${N_t}^{3+} + {N_c}^{2+} + O^+$ (3,2,1) channels, as well as N_2O^{7+} into the ${N_t}^{3+} + {N_c}^{2+} + O^{2+}$ (3,2,2) and ${N_t}^{2+} + {N_c}^{3+} + O^{2+}$ (2,3,2) channels are evaluated by putting a similar condition on the Dalitz plots. For these two cases the CE predicted that values be relatively close to each other (see Table I) and the difference in the experimental spectra are not very clear. Moreover, the experimental KER spectra show some difference for these channels as expected by the CE model. For these channels the experimental branching ratios are (3,2,1) : (2,3,1) = 0.732 : 0.268, and (3,2,2) : (2,3,2) = 0.753 : 0.247.

IV. CONCLUSION

In conclusion, we studied the three-body breakup dynamics of N_2O^{q+} ($3 \leqslant q \leqslant 7$) upon the impact of highly charged heavy ions (Ar^{8+} and Xe^{15+}). The KER distributions for different fragmentation channels are derived and compared with available experimental and theoretical data wherever possible. Furthermore, the projectile-charge-state dependence is also studied. It is found that, for a few channels, the width of the KER spectra has a mild dependence on the projectile charge states, which contradicts the spectra observed by Werner *et al.* for high-energy projectiles [30]. In the present work we have, furthermore, investigated the concerted and sequential decay mechanisms in three-body decay of N_2O^{q+} by using Dalitz plots and Newton diagrams. Thereby, a sequential decay channel has been observed for the breakup of N_2O^{3+} and N_2O^{4+} where the existence of an intermediate metastable NO^{2+} is noticed. Additionally, the KER spectra as well as branching ratios of different mutually mixed decay channels of N_2O^{q+}, for $4 \leqslant q \leqslant 7$, have been deduced by using the Dalitz plot technique. These spectra have been compared with predictions of the CE model and qualitatively good agreement is observed.

ACKNOWLEDGMENTS

We acknowledge K. V. Thulasiram and W. A. Fernandes for their scientific and technical support during ECR operation.

[1] J. D. Savee, V. A. Mozhayskiy, J. E. Mann, A. I. Krylov, and R. E. Continetti, Science **321**, 826 (2008).

[2] N. Neumann, D. Hant, L. P. H. Schmidt, J. Titze, T. Jahnke, A. Czasch, M. S. Schöffler, K. Kreidi, O. Jagutzki, H. Schmidt-Böcking, and R. Dörner, Phys. Rev. Lett. **104**, 103201 (2010).

[3] R. Guillemin, P. Decleva, M. Stener, C. Bomme, T. Marin, L. Journel, T. Marchenko, R. K. Kushawaha, K. Jänkälä, N. Trcera, K. P. Bowen, D. W. Lindle, M. N. Piancastelli, and M. Simon, Nat. Commun. **6**, 6166 (2015).

[4] A. Khan, L. C. Tribedi, and D. Misra, Phys. Rev. A **92**, 030701(R) (2015).

[5] C. Maul and K.-H. Gericke, Int. Rev. Phys. Chem. **16**, 1 (1997).

[6] S. Hsieh and J. H. D. Eland, J. Phys. B: At., Mol. Opt. Phys. **30**, 4515 (1997).

[7] J. Küpper, S. Stern, L. Holmegaard, F. Filsinger, A. Rouzée, A. Rudenko, P. Johnsson, A. V. Martin, M. Adolph, A. Aquila, S. c. v. Bajt, A. Barty, C. Bostedt, J. Bozek, C. Caleman, R. Coffee, N. Coppola, T. Delmas, S. Epp, B. Erk, L. Foucar, T. Gorkhover, L. Gumprecht, A. Hartmann, R. Hartmann, G. Hauser, P. Holl, A. Hömke, N. Kimmel, F. Krasniqi, K.-U. Kühnel, J. Maurer, M. Messerschmidt, R. Moshammer, C. Reich, B. Rudek, R. Santra, I. Schlichting, C. Schmidt, S. Schorb, J. Schulz, H. Soltau, J. C. H. Spence, D. Starodub, L. Strüder, J. Thøgersen, M. J. J. Vrakking, G. Weidenspointner, T. A. White, C. Wunderer, G. Meijer, J. Ullrich, H. Stapelfeldt, D. Rolles, and H. N. Chapman, Phys. Rev. Lett. **112**, 083002 (2014).

[8] C. E. Liekhus-Schmaltz, I. Tenney, T. Osipov, A. Sanchez-Gonzalez, N. Berrah, R. Boll, C. Bomme, C. Bostedt, J. D. Bozek, S. Carron, R. Coffee, J. Devin, B. Erk, K. R. Ferguson, R. W. Field, L. Foucar, L. J. Frasinski, J. M. Glownia, M. Gühr, A. Kamalov, J. Krzywinski, H. Li, J. P. Marangos, T. J. Martinez, B. K. McFarland, S. Miyabe, B. Murphy, A. Natan, D. Rolles, A. Rudenko, M. Siano, E. R. Simpson, L. Spector, M. Swiggers, D. Walke, S. Wang, T. Weber, P. H. Bucksbaum, and V. S. Petrovic, Nat. Commun. **6**, 8199 (2015).

[9] B. Erk, R. Boll, S. Trippel, D. Anielski, L. Foucar, B. Rudek, S. W. Epp, R. Coffee, S. Carron, S. Schorb, K. R. Ferguson, M. Swiggers, J. D. Bozek, M. Simon, T. Marchenko, J. Küpper, I. Schlichting, J. Ullrich, C. Bostedt, D. Rolles, and A. Rudenko, Science **345**, 288 (2014).

[10] A. Hishikawa, E. J. Takahashi, and A. Matsuda, Phys. Rev. Lett. **97**, 243002 (2006).

[11] M. Pitzer, M. Kunitski, A. S. Johnson, T. Jahnke, H. Sann, F. Sturm, L. P. H. Schmidt, H. Schmidt-Böcking, R. Dörner, J. Stohner, J. Kiedrowski, M. Reggelin, S. Marquardt, A. Schießer, R. Berger, and M. S. Schöffler, Science **341**, 1096 (2013).

[12] X. Xie, E. Lötstedt, S. Roither, M. Schöffler, D. Kartashov, K. Midorikawa, A. Baltuška, K. Yamanouchi, and M. Kitzler, Sci. Rep. **5**, 12877 (2015).

[13] U. Werner, N. M. Kabachnik, V. N. Kondratyev, and H. O. Lutz, Phys. Rev. Lett. **79**, 1662 (1997).

[14] A. Hishikawa, H. Hasegawa, and K. Yamanouchi, Chem. Phys. Lett. **361**, 245 (2002).

[15] F. Légaré, K. F. Lee, I. V. Litvinyuk, P. W. Dooley, S. S. Wesolowski, P. R. Bunker, P. Dombi, F. Krausz, A. D. Bandrauk, D. M. Villeneuve, and P. B. Corkum, Phys. Rev. A **71**, 013415 (2005).

[16] B. Wales, T. Motojima, J. Matsumoto, Z. Long, W.-K. Liu, H. Shiromaru, and J. Sanderson, J. Phys. B: At., Mol. Opt. Phys. **45**, 045205 (2012).

[17] A. Matsuda, M. Fushitani, R. D. Thomas, V. Zhaunerchyk, and A. Hishikawa, J. Phys. Chem. A **113**, 2254 (2009).

[18] M. Alagia, P. Candori, S. Falcinelli, M. Lavollée, F. Pirani, R. Richter, S. Stranges, and F. Vecchiocattivi, Chem. Phys. Lett. **432**, 398 (2006).

[19] L. Ferrand-Tanaka, M. Simon, R. Thissen, M. Lavollée, and P. Morin, Rev. Sci. Instrum. **67**, 358 (1996).

[20] R. Murphy and W. Eberhardt, J. Chem. Phys. **89**, 4054 (1988).

[21] N. A. Love and S. D. Price, Phys. Chem. Chem. Phys. **6**, 4558 (2004).

[22] P. Bhatt, R. Singh, N. Yadav, and R. Shanker, Phys. Rev. A **86**, 052708 (2012).

[23] A. Khan and D. Misra, J. Phys. B: At., Mol. Opt. Phys. **49**, 055201 (2016).

[24] B. Siegmann, U. Werner, H. Lutz, and R. Mann, in *GSI Scientific Report 2002*, p. 100 (GSI, Darmstadt, 2003).

[25] X. Zhou, P. Ranitovic, C. W. Hogle, J. H. D. Eland, H. C. Kapteyn, and M. M. Murnane, Nat. Phys. **8**, 232 (2012).

[26] L. Frasinski, P. Hatherly, and K. Codling, Phys. Lett. A **156**, 227 (1991).

[27] A. Hishikawa, A. Iwamae, K. Hoshina, M. Kono, and K. Yamanouchi, Res. Chem. Intermed. **24**, 765 (1998).

[28] M. Ueyama, H. Hasegawa, A. Hishikawa, and K. Yamanouchi, J. Chem. Phys. **123**, 154305 (2005).

[29] R. Karimi, É. Bisson, B. Wales, S. Beaulieu, M. Giguère, Z. Long, W.-K. Liu, J.-C. Kieffer, F. Légaré, and J. Sanderson, J. Chem. Phys. **138**, 204311 (2013).

[30] U. Werner, B. Siegmann, and R. Mann, in *GSI Scientific Report 2006*, p. 253 (GSI, Darmstadt, 2007).

[31] A. Khan, L. C. Tribedi, and D. Misra, Rev. Sci. Instrum. **86**, 043105 (2015).

[32] A. N. Agnihotri, A. H. Kelkar, S. Kasthurirangan, K. V. Thulasiram, C. A. Desai, W. A. Fernandez, and L. C. Tribedi, Phys. Scr. **2011**, 014038 (2011).

[33] Roentdek handels gmbh, http://www.roentdek.com/.

[34] I. Ben-Itzhak, S. G. Ginther, V. Krishnamurthi, and K. D. Carnes, Phys. Rev. A **51**, 391 (1995).

[35] E. Wells, V. Krishnamurthi, K. D. Carnes, N. G. Johnson, H. D. Baxter, D. Moore, K. M. Bloom, B. M. Barnes, H. Tawara, and I. Ben-Itzhak, Phys. Rev. A **72**, 022726 (2005).

[36] R. Dalitz, Philos. Mag. **44**, 1068 (1953).

[37] T. Masuoka, J. Chem. Phys. **100**, 6422 (1994).

[38] R. Baková, J. Fišer, T. Šedivcová-Uhlíková, and V. Špirko, J. Chem. Phys. **128**, 144301 (2008).

[39] D. Edvardsson, M. Lundqvist, P. Baltzer, B. Wannberg, and S. Lunell, Chem. Phys. Lett. **256**, 341 (1996).

[40] H. O. Folkerts, R. Hoekstra, and R. Morgenstern, Phys. Rev. Lett. **77**, 3339 (1996).

[41] M. Ehrich, B. Siegmann, U. Werner, and H. Lebius, Radiat. Phys. Chem. **68**, 127 (2003).